



ELSEVIER

1 December 1998

OPTICS  
COMMUNICATIONS

Optics Communications 157 (1998) 282–290

Full length article

# Cleaving optical fibre lengths to high relative accuracy

Mark P.J.L. Chang, David F. Buscher

*Rochester Building, Physics Department, Durham University, South Road, Durham DH1 3LE, UK*

Received 7 May 1998; revised 5 August 1998; accepted 10 August 1998

---

## Abstract

Single-mode fibres are an important component in systems such as ground-based stellar interferometers. A major drawback in using them is the large optical path differences that arise between individual fibres, due to the difficulty in equalising their lengths. The tolerances on fibre length differences are calculated for broadband interferometry in terms of the fringe visibility. A simple technique for producing short (between 1 and 2.75 m) lengths of single-mode silica waveguides with a mean relative accuracy of  $2.28 \pm 1.53 \mu\text{m}$  and of optically measuring these length differences is described herein. © 1998 Elsevier Science B.V. All rights reserved.

*Keywords:* Single mode fibres; Broadband interferometry; Optical fibre length tolerance

---

## 1. Introduction

A major development in modern stellar interferometry is the incorporation of single-mode (SM) guided optics [1]. The advantage afforded by these components is their perfect spatial filtering of atmospherically aberrated wavefronts. An estimate of the fringe visibility can then be made which is independent of atmospheric perturbations and as a result, the accuracy on object visibility measurements is increased by at least an order of magnitude [2,3]. A test-bed visible region stellar interferometer using tapered, SM optical fibres [4] is currently being developed at Durham.

The inherent dispersive property of any dielectric waveguide is a drawback of guided optics since it essentially limits the transmissible bandwidth. A broadband interferometric instrument based on such waveguides is sensitive to length differences between its arms which induce extra chromatic dispersion, lowering the fringe contrast. So to effectively design and use a broadband interferometer requires the minimisation of this dispersion. Active compensation schemes have been described [6,7], but none of these methods exactly cancels the effect of the excess waveguide section, especially if it is a significant quantity. Clearly the most desirable starting point is to equalise the length of the waveguides in each arm.

Concerning the issue of coupling starlight into fibre waveguides, it is necessary to have diffraction-limited spots incident on the input aperture. Since standard SM fibres have fast f-ratios, the input coupling becomes non-trivial. That is to say, from the point of view of the incoming wavefronts, a low value f-ratio is required to match the SM fibre fundamental mode field radius. One method we have proposed to alleviate this is to employ adiabatically tapered, SM fibres in stellar interferometry. The taper acts as a lossless self-aligned lens which decreases the fibre's f-ratio, thereby simplifying the input coupling.

For a high contrast fringe signal, when observing sources with wide bandwidths (eg.  $\Delta\lambda = 300 \text{ nm}$ ) at short wavelengths, the tolerance on the relative length difference between fibre arms can be severe. In Section 2, we deduce an expression relating the length difference  $\Delta L$  to the fringe modulation as a function of the observed frequency and bandwidth. The results given by expression are in agreement with simulations produced by Shaklan [5] and serve as a guide to the tolerances required to achieve a given fringe modulation depth.

Burnett and Jones [8] demonstrated that fibres could be cleaved with a mean relative accuracy of  $10.8 \mu\text{m}$ . However, their proposed method required that both ends of the fibre be cleaved, which is not desirable for tapered SM

fibres due to the fibre production method. Tapered fibres are fabricated with specified taper (large) and normal (small) core radii, so cleaving the tapered end evidently alters the taper core radius. In Section 4 we describe an accurate method for producing equal length optical fibres by cleaving only one end and an optical technique for determining the residual length difference with respect to a reference fibre.

**2. Tolerance on length difference**

Consider an optical fibre waveguide illuminated by a time dependent signal from an astronomical source. The incident scalar field, written as a Fourier expansion in terms of angular frequency  $\omega$ , is

$$E_{in}(t) = \int_{-\infty}^{+\infty} E(\omega)\exp(-2\pi i \omega t) d\omega. \tag{1}$$

The output field, after propagation through the waveguide, can be expressed as

$$E_{out}(t) = \int_{-\infty}^{+\infty} E(\omega)\exp[-i(\omega t + \Phi(\omega))] d\omega. \tag{2}$$

The induced phase change  $\Phi(\omega)$  can be expressed as the sum of a dispersive material component and an air path component. The material contribution  $\Phi_m$  can be approximated by a Taylor expansion

$$\Phi_m \approx \beta L + (\omega - \omega_0) \frac{d\beta}{d\omega} L + \frac{(\omega - \omega_0)^2}{2} \frac{d^2\beta}{d\omega^2} L, \tag{3}$$

with  $\omega_0$  the centre frequency and  $L$  the length of the fibre. The propagation constant of the fibre waveguide is the conventional  $\beta \triangleq \kappa n$  where  $\kappa$  is the vacuum wavenumber and  $n$  the fibre refractive index. This expression is valid for SM fibres operating in the visible region, where the effects of waveguide geometry and refractive index profile delays are negligible. The air path contribution  $\Phi_a$  can be written as

$$\Phi_a = \omega \{ x_v + x_a [1 + N_a(\omega)] \}, \tag{4}$$

where  $x_v$  is the path in vacuum,  $x_a$  is the path length in air and  $[1 + N_a(\omega)]$  is the index of refraction of air.

We now refer to the schematic two fibre, single baseline interferometer shown in Fig. 1. The coupling is assumed to be perfect for both waveguides and their material dispersion functions are taken to be exactly the same. The light is guided to a recombination plane where a detector

produces a signal linearly proportional to the intensity of the recombined beam. In the shorter arm, the missing thickness of dispersive material is compensated for by an additional air path. For a zero group delay position, the linear parts of the material and air contributions to the induced phase cancel. We are then left with a second order induced phase shift

$$\Delta\Phi = \frac{(\Delta\omega)^2}{2} \frac{d^2\beta}{d\omega^2} \Delta L + \text{const}, \tag{5}$$

where  $\Delta\omega$  is the angular frequency bandwidth and  $d^2\beta/d\omega^2$  is the chromatic dispersion. It should be noted that we neglect path fluctuations caused by air turbulence and any wavelength dependence of the visibility phase. It is also assumed that field-of-view path length differences are unimportant.

It is generally assumed that the condition  $\Delta\Phi \leq \pi$  should be satisfied to produce a signal modulation at the output. That is to say, the recombining fields have a phase lag of less than half a wave. This gives the maximum tolerance for standard fused silica fibres operating in the astronomical V-band ( $\lambda_c = 0.55 \mu\text{m}$ ,  $\Delta\lambda/\lambda = 0.16$ ) to be  $71.85 \mu\text{m}$ .

A more stringent and practical tolerance can be derived from the following considerations. It is well known that the character of an interferogram formed from a point source is determined by the complex degree of coherence  $\gamma(\tau)$ . This is the normalised form of the self coherence (autocorrelation) function  $\Gamma(\tau)$ . It can be shown [10,11] that  $|\gamma(\tau)|$  is the same as the fringe contrast  $V$ , defined as

$$V \triangleq \frac{I_{max} - I_{min}}{I_{max} + I_{min}} \tag{6}$$

for an interferometer with equal transmission in both arms. For a stationary random process  $\gamma(\tau)$  is a Fourier Transform (FT) of the normalised source power spectral density  $G$

$$\gamma(\tau) = \int_0^\infty G(\nu)\exp(-2\pi i \nu \tau) d\nu. \tag{7}$$

While this expression is true for a perfect instrument, in all practical cases the ideal visibility is always modified by the instrumental transfer function  $T_i(\nu)$ ,

$$\gamma(\tau) = \int_0^\infty T_i(\nu)G(\nu)\exp(-2\pi i \nu \tau) d\nu. \tag{8}$$

We assume that the shape of the normalised source power

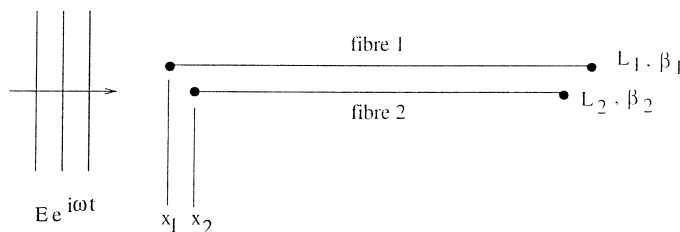


Fig. 1. Idealised two SM fibre interferometer illuminated by a point source.

spectrum is approximately Gaussian so it may be written as

$$G(\nu) = \frac{2A}{\Delta\nu\sqrt{\pi}} \exp\left(-\left(A \frac{\nu - \nu_0}{\Delta\nu}\right)^2\right). \quad (9)$$

$\Delta\nu$  denotes the frequency bandwidth and  $A = 2\sqrt{\ln 2}$ . Eqs. (3) and (4) indicate that the transmission function can be written (in terms of  $\nu$ ) as

$$T_i(\nu) = \exp(-i\Phi) = \exp\left(-i\Delta L \left( \beta + (\nu - \nu_0)\beta_{\nu} + \frac{(\nu - \nu_0)^2}{2}\beta_{\nu\nu} + \nu x_a [1 + N_a(\nu)] \right)\right), \quad (10)$$

where  $\beta_{\nu} = d\beta/d\nu$  and  $\beta_{\nu\nu} = d^2\beta/d\nu^2$ . It is assumed that the additional air path in this interferometric system is very much less than a metre; since  $x_v$  and  $x_a$  typically differ by less than 300  $\mu\text{m}/\text{m}$  of path length it is valid to neglect the sum of the air and vacuum paths. Adjusting the system air paths to remove the linear terms allows us to write

$$\gamma(\tau) = \frac{2A}{\Delta\nu\sqrt{\pi}} \int_0^{\infty} \exp\left(-\left(\frac{A^2}{\Delta\nu^2} + \frac{i\Delta L}{2}\beta_{\nu\nu}\right)(\nu - \nu_0)^2 + 2\pi i(\nu - \nu_0)\tau\right) d\nu. \quad (11)$$

We find

$$\gamma(\tau) = \left(\frac{A}{\Delta\nu}\right) \frac{1}{(\xi + i\eta)^{1/2}} \exp\left(-\frac{(\pi\tau)^2}{(\xi + i\eta)^{1/2}}\right), \quad (12)$$

where  $\xi \triangleq (A/\Delta\nu)^2$  and  $\eta \triangleq (\Delta L/2)\beta_{\nu\nu}$ . The modulus of Eq. (12) is

$$|\gamma(\tau)| = \left(\frac{A}{\Delta\nu}\right) \frac{1}{(\xi^2 + \eta^2)^{1/4}} \times \exp\left(-(\pi\tau)^2 \Re\left(\frac{\xi - i\eta}{\xi^2 + \eta^2/4}\right)\right), \quad (13)$$

where  $\Re$  shows that the real part of the expression should be taken. We are concerned with the variation of the visibility function at the zero group delay position ( $\tau = 0$ ), so

$$V = \left(\frac{A}{\Delta\nu}\right) \left[ \left(\frac{A}{\Delta\nu}\right)^4 + \left(\frac{\Delta L\beta_{\nu\nu}}{2}\right)^2 \right]^{-1/4}. \quad (14)$$

It is now possible to impose a condition of minimum visibility  $V_{\min}$ . Therefore  $V \geq V_{\min}$  which gives

$$\Delta L \leq \frac{2}{\beta_{\nu\nu}} \left[ \left(\frac{A}{\Delta\nu V_{\min}}\right)^4 - \left(\frac{A}{\Delta\nu}\right)^4 \right]^{1/2}. \quad (15)$$

The calculated values for the constraints on the optical path difference of single-mode silica fibres are shown in Figs. 2 and 3.

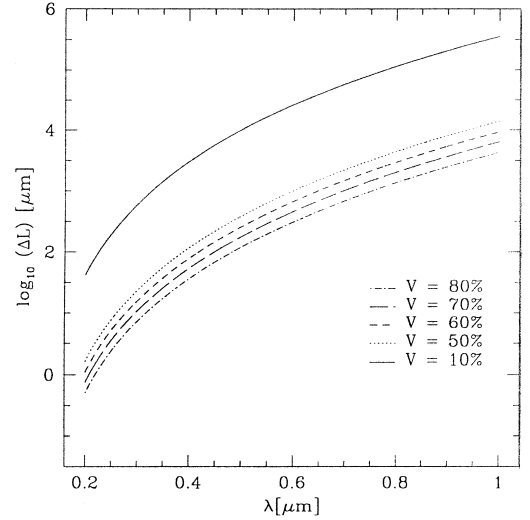


Fig. 2. Tolerance on fibre lengths for a source bandwidth of  $\Delta\lambda = 0.1 \mu\text{m}$  as a function of wavelength, for various visibility  $V$  criteria.

Let  $V_{\min} \geq 0.8$ , which is equivalent to the classical Strehl criterion of diffraction limited imaging. In this case the relative fibre length tolerance for a source of 100 nm bandwidth, centered on 633 nm is  $\Delta L \leq 410 \mu\text{m}$ . For a source of  $\Delta\lambda = 300 \text{ nm}$  centered on 633 nm, the tolerance is  $\Delta L \leq 41 \mu\text{m}$ . The value of  $\beta_{\nu\nu}$  at 633 nm is  $2.869 \text{ ps}^2 \text{ m}^{-1}$ .

For a more relaxed constraint  $V_{\min} \geq 0.5$ , the maximum allowable values of  $\Delta L$  are  $1325 \mu\text{m}$  and  $132 \mu\text{m}$  respectively, with the same sources as before.

The two plots in Fig. 4 illustrate the degradation in fringe visibility as a function of  $\Delta L$  for two specific wavelengths,  $\lambda = 633 \text{ nm}$  and  $\lambda = 1 \mu\text{m}$ .

### 3. Fibre induced phase

The aim of this section is to quantify the relationship between fibre dispersion and interferometric phase measurements. By doing so, it will be shown that the length difference between any two fibres may be found from the fringe visibility curve.

We have seen that the chromatic dispersion  $D$  can be expressed as

$$D \triangleq \frac{d^2\beta}{d\omega^2} = \frac{1}{c^2} \frac{d^2\beta}{d\kappa^2}. \quad (16)$$

Recall Eq. (5) for the phase difference between fields in the recombination plane.  $\Delta\Phi(\kappa)$  is not a useful observable since it is non-trivial to calibrate for the constant term. Considering the first differential with respect to wavenumber  $d\Delta\Phi(\kappa)/d\kappa$  is also ambiguous since it too includes a constant relating to a linear translation of the interfero-

gram. The quantity which is of use is the second order differential with respect to  $\kappa$ . This can be regarded as the phase curvature and is found to be

$$\frac{d^2\Delta\Phi(\kappa)}{d\kappa^2} = \frac{d^2\beta}{d\kappa^2}\Delta L. \quad (17)$$

The higher order terms are not relevant to this approximation so have been neglected.

We now have

$$\frac{d^2\Delta\Phi(\kappa)}{d\kappa^2} = c^2\Delta LD \quad (18)$$

or equivalently

$$\Delta L = \Delta\Phi_{\lambda\lambda}/\beta_{\lambda\lambda}, \quad (19)$$

which means that the length difference between fibre arms

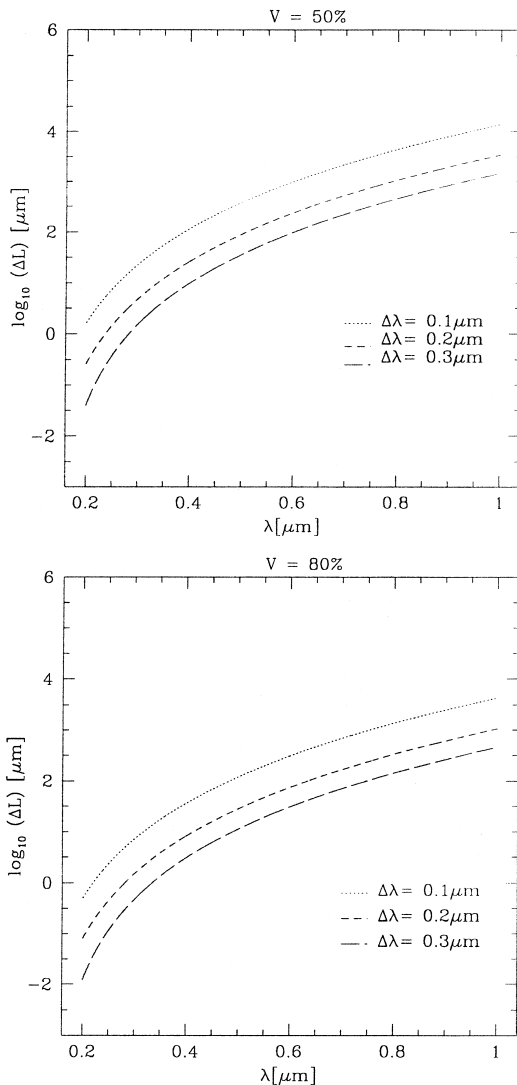


Fig. 3. Tolerance on fibre lengths for (top)  $V = 0.5$  and (bottom)  $V = 0.8$  for source bandwidths  $\Delta\lambda = 0.1 \mu\text{m}$ ,  $\Delta\lambda = 0.2 \mu\text{m}$  and  $\Delta\lambda = 0.3 \mu\text{m}$ .

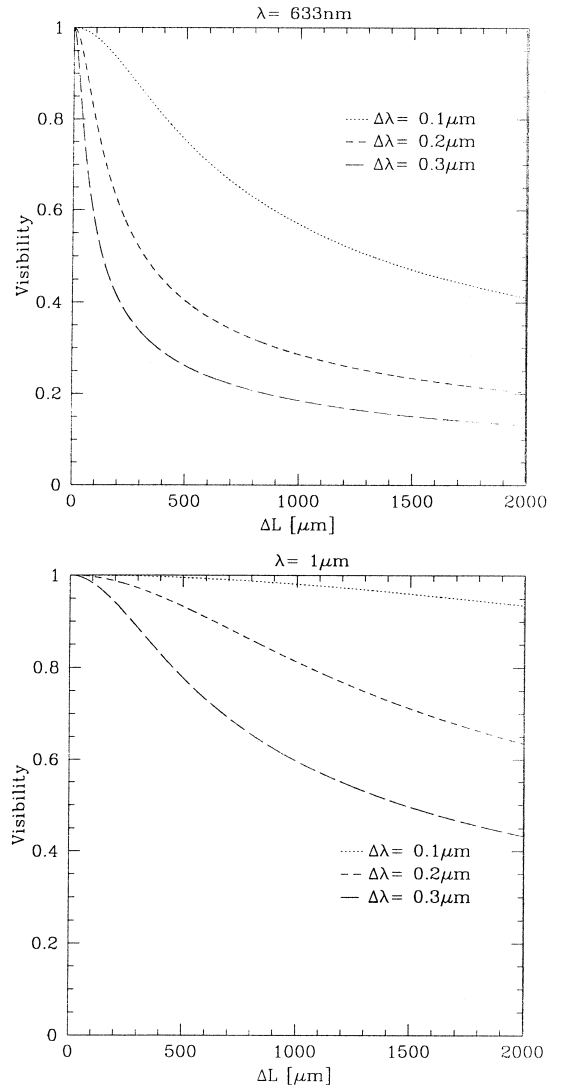


Fig. 4. Fringe visibility as a function of fibre length difference  $\Delta L$  (top) for  $\lambda = 0.633 \mu\text{m}$  and (bottom)  $\lambda = 1 \mu\text{m}$ .

can be deduced from the second differential of induced phase with respect to wavelength, provided that the fibres are made of the same material. The abbreviations  $\beta_{\lambda\lambda} = d^2\beta(\lambda)/d\lambda^2$  and  $\Delta\Phi_{\lambda\lambda} = d^2\Delta\Phi(\lambda)/d\lambda^2$  have been used. The functional form of  $\beta_{\lambda\lambda}$  is

$$\beta_{\lambda\lambda} = \frac{4\pi}{\lambda^3}n - \frac{4\pi}{\lambda^2}\frac{dn}{d\lambda} + \frac{2\pi}{\lambda}\frac{d^2n}{d\lambda^2}. \quad (20)$$

The refractive index function is given by the Sellmeier equation

$$n^2 - 1 = \frac{a_1\lambda^2}{\lambda^2 - b_1} + \frac{a_2\lambda^2}{\lambda^2 - b_2} + \frac{a_3\lambda^2}{\lambda^2 - b_3}, \quad (21)$$

Table 1  
Sellmeier constants for pure fused silica

$a_1$	0.6961663	$b_1$	0.004679148
$a_2$	0.4079426	$b_2$	0.01351206
$a_3$	0.8974994	$b_3$	97.934002

so that

$$\frac{dn}{d\lambda} = -\frac{\lambda}{n} \left[ \frac{a_1 b_1}{(\lambda^2 - b_1)^2} + \frac{a_2 b_2}{(\lambda^2 - b_2)^2} + \frac{a_3 b_3}{(\lambda^2 - b_3)^2} \right] \quad (22)$$

and

$$\frac{d^2n}{d\lambda^2} = -\frac{4\lambda^2}{n} \left[ \frac{a_1 b_1}{(\lambda^2 - b_1)^3} + \frac{a_2 b_2}{(\lambda^2 - b_2)^3} + \frac{a_3 b_3}{(\lambda^2 - b_3)^3} \right] + \frac{1}{\lambda} \frac{dn}{d\lambda} - \frac{1}{n} \left( \frac{dn}{d\lambda} \right)^2 \quad (23)$$

As the dopants of SM fibres do not affect the refractive indices significantly, the difference between the core and cladding being typically  $\sim 10^{-3}$ , the Sellmeier constants for pure fused silica were used [12], given in Table 1. Eq. (19) thus served as the principle of the experiments described here.

The main simplification in the above model has been to neglect the effects of polarisation upon the fringe visibility. If the recombination signal is not separated in terms of its polarisation components, the detector records the vector sum of the intensity modulations. Any differential phase

delays between polarisations degrade the amplitude of the visibility signal, and can completely corrupt its phase information. So, clearly, polarisation states in the system must be well controlled. This was achieved by using commercially available fibre polarisation controllers (Lefèvre loops or Mickey ears). These operate on the basis that bending induces birefringence in the dielectric waveguide [9,13].

Although the core/cladding diameters and doping levels of real SM fibres do vary, within manufacturing tolerances, it is not necessary to account for these effects. This is apparent if we consider the propagation constant  $\beta$  within the weak guidance approximation [14],

$$\beta \approx \kappa n_{\text{clad}}(1 + B\Delta). \quad (24)$$

Here  $n_{\text{clad}}$  is the refractive index of the fibre cladding.  $B$  denotes the normalised propagation constant, varying between 0 and 1, which is independent of the refractive indices. It is clear that the product  $B\Delta \ll 1$ , so any variations will be negligible from the point of view of dispersion.

### 4. Experiment

#### 4.1. Fibre cleaving

As already mentioned, previous work [8] has demonstrated that it is possible to produce short (nominally 1.5 m) lengths of fibre to a relative accuracy of 10.8  $\mu\text{m}$ . The method required that the fibres be clamped at their midpoints on a stable mounting block. With the cleave tool situated at one end of the optical table, a fibre was

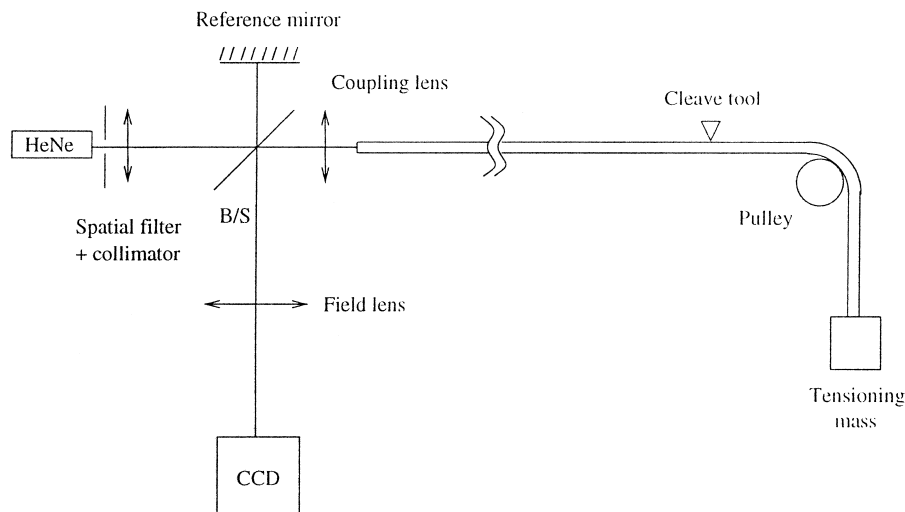


Fig. 5. Cleaving method. The datum end is a classical Twyman-Green interferometer illuminated by a spatially filtered HeNe laser. It also serves to measure the fibre endface quality.

stretched across the tool and tensioned by a small mass. Upon cleaving, the clamp was rotated and the other end of the fibre was prepared in the same way. The accuracy is therefore dependent on the reproducibility of both the fibre catenary (from clamp to cleave tool) and the clamp positioning.

Our technique is based on providing a datum position for one endface and cleaving the other side of the fibre. The principal variable is therefore the reproducibility of the catenary. For standard 125  $\mu\text{m}$  fibres whose outer diameters (even including the buffer) are constant to within a few microns along the length of the fibre, the catenaries are easy to reproduce accurately. Tapered fibres, due to the manufacturing process, have larger outer diameters at the tapered endface than at the normal end. This can lead to a decrease in flexibility of the fibre, so requiring more care when tensioning the fibre.

The optical fibres used were standard silica with a cladding diameter of 125  $\mu\text{m}$  and a mean acrylate buffer diameter of 300  $\mu\text{m}$  provided by Oxford Electronics.

One (flat) endface of the fibre served as the test component in a Twyman-Green interferometer, illustrated in Fig. 5. The fibre was clamped in PTFE jaws, so as not to deform the buffer coating, since this ultimately deteriorates the transmission performance.

The interferometer was illuminated by a spatially filtered, collimated HeNe laser, and the light focused through a  $\times 10$  microscope objective onto the fibre endface. The detector was a standard television CCD. A small mass was attached to the other end of the fibre, which was stretched over the cleaving unit and a pulley. The monomer acrylate buffer was removed from that end prior to cleaving, and the exposed fibre thoroughly wetted to counter any static charge. A York FK11 fibre cleaver was used.

After finding the interference fringes in the viewing plane of the Twyman-Green, the reference end was positioned such that the central circular fringe filled the detec-

tor's field-of-view. This is clearly the focal point of the objective which acted as the datum for all the fibres. Again care was taken to align the fibre endface on axis with respect to the microscope objective in order to minimise the effects of coma.

The fibre was clamped down in the cleaver so as not to significantly alter the shape of its catenary. Misalignments of the fibre position from the pulley to the datum also have to be kept to a minimum. The mass was removed from the fibre before cleaving.

#### 4.2. OPD measurement

A Mach-Zehnder interferometer illuminated by a reference laser diode and a tungsten source was used to determine the length difference between any given fibre pair, as shown in Fig. 6.

Initially the inputs of the fibre pair were aligned with a travelling microscope such that the image of one endface overlapped the position of the other. Since the positional tolerance of the core within the cladding is very high, this alignment was sufficient to locate the cores in the transverse ( $x$ - $y$ ) directions. The interferometer was illuminated with a 0.3 mW laser diode, operating above its threshold current. Prior to overlapping the output beams, a polariser  $P_1$  was placed in front of the laser source and an analyser  $P_2$  in front of the detector. They were oriented with their polarisation axes perpendicular to each other. The polarisation controllers  $PC_1$  and  $PC_2$  were individually adjusted by altering the angle of each "Mickey ear" to minimize the throughput. Although for a wide bandwidth source there is some residual polarisation leakage, this is not an issue since this is less than 1%.

With the axes of  $P_1$  and  $P_2$  parallel, the fibre outputs were aligned to form tilt fringes at the recombination plane. Reducing the current to just below threshold increased the spectral bandwidth (to the maximum width of

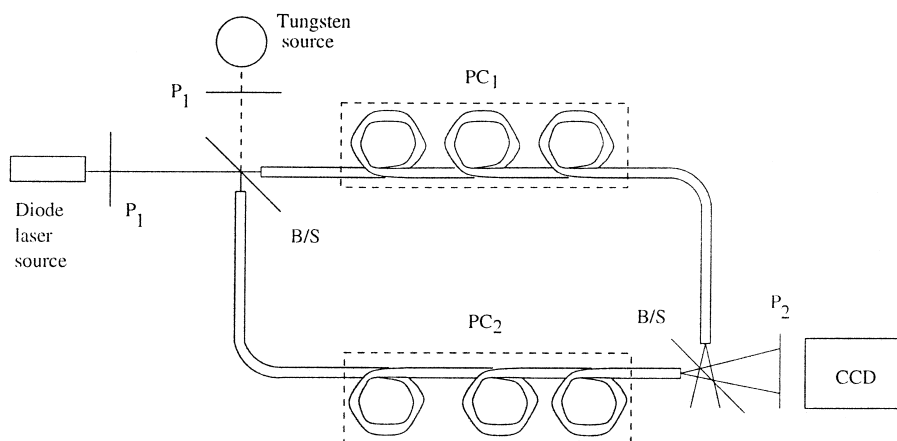


Fig. 6. The fibre lengths were measured with a white light fibre Mach-Zehnder interferometer. Polarisation control was achieved by looping the fibres ( $PC_{1,2}$ ). Polarisers  $P_1$  and  $P_2$  were oriented such that their axes were parallel during the measurements. See text for details.

the laser gain envelope), so decreasing the coherence length to about 100  $\mu\text{m}$ . This helped to locate the white light fringe position in the transverse ( $z$ ) direction. See Fig. 7.

The broadband fringes formed with the tungsten source were recorded with a Cohu CCD camera attached to a frame grabber. CCD images of the laser source provided the reference wavenumber. To improve the signal-to-noise ratio, good background subtraction was necessary. The background for the laser source was measured by coadding ten frames with a fringe signal. The visibility phase was offset by a small amount between frames by moving a

fibre output along the  $z$  axis. The white light background was obtained by offsetting an output along the  $z$  axis until the fringes were out of the field of view.

The visibility curve of the background subtracted laser interference pattern was calculated by an inverse 2D Fourier transformation. By identifying its peak position, the wavenumber calibration in terms of the Fourier plane could be extracted.

The amplitude and phase of the background subtracted white light visibility curve was then calculated. Clearly, the phase produced can have a  $2\pi$  ambiguity since it is the argument of the real and imaginary parts of the FTs. For

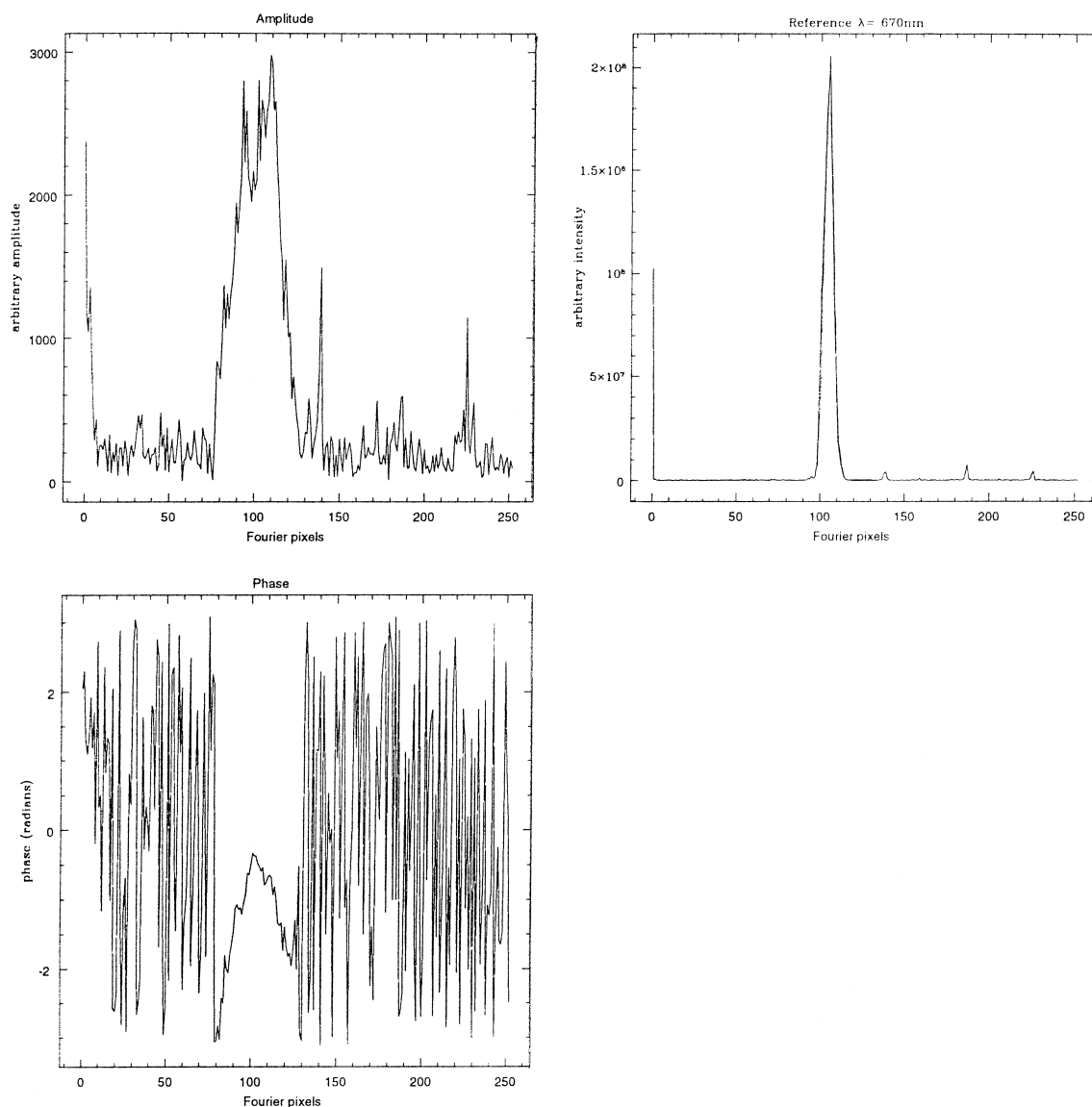


Fig. 7. Interferogram amplitude and phase from the white light fibre Mach-Zehnder and its corresponding wavelength reference power spectrum.

Table 2

Results of fibre cleaving trials. Fibres 1 to 6 were cleaved to be nominally 1.13 m, while 7 and 8 were 2.75 m in length. The values in parentheses of  $\Delta\Phi_{\lambda\lambda}$  and  $\Delta L$  use the bandwidth common to all measurements (0.466 to 0.709  $\mu\text{m}$ ) where  $\beta_{\lambda\lambda} = 96.971 \mu\text{m}^{-3}$

Fibre pair	Bandwidth (endpoints) [ $\mu\text{m}$ ]	$\beta_{\lambda\lambda}$ [ $\mu\text{m}^{-3}$ ]	$\Delta\Phi_{\lambda\lambda}$ [ $\mu\text{m}^{-2}$ ]	$\Delta L$ [ $\mu\text{m}$ ]
1,2	0.318 (0.452 to 0.771)	87.917	-143.059 (-163.842)	-1.63 (-1.69)
1,3	0.300 (0.462 to 0.762)	87.0162	-228.388 (-227.858)	-2.62 (-2.35)
1,4	0.379 (0.466 to 0.845)	70.9102	-145.098 (-124.675)	-2.05 (-1.29)
1,5	0.415 (0.383 to 0.798)	103.915	-148.887 (-194.094)	-1.43 (-2.00)
1,6	0.429 (0.322 to 0.750)	145.544	-457.414 (-336.058)	-3.14 (-3.47)
2,3	0.346 (0.432 to 0.778)	92.1566	-337.044 (-334.508)	-3.66 (-3.45)
2,4	0.355 (0.394 to 0.749)	111.551	-149.824 (-113.699)	-1.34 (-1.17)
2,5	0.437 (0.379 to 0.816)	101.328	-178.072 (-141.738)	-1.76 (-1.46)
2,6	0.335 (0.412 to 0.747)	105.289	-303.544 (-344.210)	-2.88 (-3.55)
7,8	0.276 (0.434 to 0.709)	107.484	-119.327 (-141.704)	-1.11 (-1.46)

the more highly dispersed interferograms it was necessary to unwrap the phase information. The full width at half maximum of the amplitude data was required to constrain the region of phase data which was unwrapped. A second order polynomial fit was then applied to the phase data. From this was obtained the mean curvature  $\Delta\Phi_{\lambda\lambda}$  over the detected bandwidth.

The value of  $\beta_{\lambda\lambda}$  was calculated by fitting a second order polynomial to  $\beta$  for the measured bandwidth.  $\Delta L$  was then found using Eq. (19).

Six fibres of nominally 1.13 m in length were produced of which 9 pairs were measured as described. The results are given in Table 2. The mean accuracy for cleaving fibres of nominal length 1.13 m can be seen to be  $-2.28 \mu\text{m}$ , with a standard deviation  $\sigma$  of  $0.78 \mu\text{m}$ . The band-

pass endpoints and thus the bandwidth variations shown are due to a combination of signal to noise considerations and calibration errors. Fibres of nominally 2.75 m were also produced to high accuracy, the maximum length being limited only by the optical table.

The accuracy of the wavelength calibration affects the accuracy of the bandwidth determination. The values of the fitted  $\beta_{\lambda\lambda}$  can be related to a central  $\lambda$  for the tungsten source throughput; we find a mean detected wavelength  $\langle \lambda \rangle = 0.576 \mu\text{m}$  and a standard deviation  $\sigma_{\lambda} = 0.033 \mu\text{m}$ . Even assuming the calibration is perfect, it is natural to expect that the detected bandwidths for different pairs of fibres will not be equal for a given signal-to-noise ratio. This is because of the transmission bandwidth limitation imposed by chromatic dispersion effects.

Table 3

Results of ‘‘closed loop’’ measurements for Table 2. The loop error is defined as  $\epsilon = (\Delta L_{ij} - \Delta L_{ik}) + \Delta L_{jk}$ . The values in parentheses refer to the common bandwidth results

Fibre triple	$i$	$j$	$k$	$\Delta L_{ij}$ [ $\mu\text{m}$ ]	$\Delta L_{ik}$ [ $\mu\text{m}$ ]	$\Delta L_{jk}$ [ $\mu\text{m}$ ]	$\epsilon$ [ $\mu\text{m}$ ]
	1	2	3	-1.63 (-1.69)	-2.62 (-2.35)	-3.66 (-3.45)	-2.67 (-2.79)
	1	2	4	-1.63 (-1.69)	-2.05 (-1.29)	-1.34 (-1.17)	-0.92 (-1.57)
	1	2	5	-1.63 (-1.69)	-1.43 (-2.00)	-1.76 (-1.46)	-1.96 (-1.15)
	1	2	6	-1.63 (-1.69)	-3.14 (-3.47)	-2.88 (-3.55)	-1.37 (-1.77)

To check the calibration accuracy, we recalculated  $\Delta L$  for the fibres using the value of  $\beta_{\lambda\lambda}$  for the detected bandwidth common to all the 1.13 m fibre pairs (0.466 to 0.709  $\mu\text{m}$ ). The results have a mean accuracy of  $-2.27 \mu\text{m}$ , with  $\sigma = 0.93 \mu\text{m}$ , which is consistent with the result found previously.

A series of ‘‘closed loop’’ comparisons were also made to determine the measurement error. That is to say, for fibres  $i, j$  and  $k$ ,  $\Delta L_{ij}$ ,  $\Delta L_{ik}$  were measured to deduce the value of  $\Delta L_{jk}$ . This was compared to measurement (Table 3), resulting in a mean closed loop errors of  $-1.73 \mu\text{m}$ ,  $\sigma = 0.65 \mu\text{m}$  for the full detected bandwidth calculation and  $-1.82 \mu\text{m}$ ,  $\sigma = 0.6 \mu\text{m}$  for the common bandwidth determination. The residual closed loop errors show that the measurements are still noise dominated, since they are not much smaller than the individual length differences.

An accuracy of 2.28  $\mu\text{m}$  is within tolerance for sources of  $\Delta\lambda = 0.3 \mu\text{m}$  centered on  $\lambda_c \approx 0.4 \mu\text{m}$ , even if the strictest criterion of  $V \geq 80\%$  is imposed. So even broadband interferometric imaging in the visible is possible with short ( $< 5 \text{ m}$ ) optical fibres. This means that, provided the input coupling to the fibres is efficient, high angular resolution spectroscopic imaging can be contemplated.

## 5. Conclusions

It is feasible to consider producing extremely accurately short lengths of tapered SM fibre, which may be used for interferometry. A simple technique for determining the relative length differences between fibres was described, allowing the calibration of systematic relative length errors between individual fibres.

The most promising result from this work has been the demonstration that ground-based interferometric spectroscopy for astronomy with SM fibres is a possibility, over and above planned interferometric imagers. Especially with the forthcoming generation of 8 m class astronomical facilities, extremely high angular resolution imaging and spectroscopy with single telescopes will soon be achievable.

## Acknowledgements

We are very grateful to Stuart Shaklan and Feng Zhao for their constructive comments on this work. MPJLC acknowledges the support of PPARC.

## References

- [1] C. Froehly, High angular resolution, in: Coherence and Interferometry through Optical Fibers, Proc. Conf. on the Scientific Importance of High Angular Resolution at IR and Optical Wavelengths, European Southern Observatory, Garching bei München, Germany, 1981, p. 285.
- [2] V.C. du Foresto, G. Perrin, J.-M. Mariotti, M. Lacasse, W. Traub, The FLUOR/IOTA fiber stellar interferometer, in: P. Kern, F. Malbet (Eds.), Integrated Optics for Astronomical Interferometry, Grenoble Observatoire de Grenoble, France, 1996, pp. 115–125.
- [3] F. Reynaud, J.J. Alleman, P. Connes, Appl. Optics 31 (1992) 3736.
- [4] M.P.J.L. Chang, D.F. Buscher, Astronomical fiber based interferometry with adaptive optics on single telescopes, in: P. Kern, F. Malbet (Eds.), Integrated Optics for Astronomical Interferometry, Grenoble, Observatoire de Grenoble, France, 1996, pp. 185–193.
- [5] S.B. Shaklan, F. Roddier, Appl. Optics 26 (1987) 2159.
- [6] D.A. Jackson, R. Priest, A. Dandridge, A.G. Tveten, Appl. Optics 19 (1980) 2926.
- [7] B.J. White, J.P. Davis, L.C. Bobb, H.D. Krumboltz, D.C. Larson, IEEE J. Lightwave Technol. LT5 (1987) 1169.
- [8] J.G. Burnett, J.D.C. Jones, Appl. Optics 16 (1992) 2977.
- [9] H.C. Lefèvre, Electron. Lett. 16 (1980) 778.
- [10] J.W. Goodman, Statistical Optics, Wiley-Interscience, New York, 1985.
- [11] M. Born, E. Wolf, Principles of Optics, Pergamon Press, New York, 1993.
- [12] S. Kobayashi, S. Shibata, N. Shibata, T. Izawa, Refractive-index dispersion of doped fused silica, in: Proc. Intern. Conf. on Integrated Optics and Optical Fibre Communication, 1977, pp. 309–312.
- [13] R. Ulrich, S.C. Rashleigh, W. Eickhoff, Optics Lett. 5 (1980) 273.
- [14] L.B. Jeunhomme, Single-Mode Fiber Optics: Principles and Applications, Marcel Dekker, New York, 1990.